



HAL
open science

A detailed experimental and kinetic modeling study on pyrolysis and oxidation of oxymethylene ether-2 (OME-2)

Kevin de Ras, Marvin Kusenberg, Guillaume Vanhove, Yann Fenard, Andreas Eschenbacher, Robin Varghese, Jeroen Aerssens, Ruben van de Vijver, Luc-Sy Tran, Joris Thybaut, et al.

► To cite this version:

Kevin de Ras, Marvin Kusenberg, Guillaume Vanhove, Yann Fenard, Andreas Eschenbacher, et al.. A detailed experimental and kinetic modeling study on pyrolysis and oxidation of oxymethylene ether-2 (OME-2). *Combustion and Flame*, 2022, 238, pp.111914. 10.1016/j.combustflame.2021.111914 . hal-03538344

HAL Id: hal-03538344

<https://hal.science/hal-03538344v1>

Submitted on 20 Oct 2022

HAL is a multi-disciplinary open access archive for the deposit and dissemination of scientific research documents, whether they are published or not. The documents may come from teaching and research institutions in France or abroad, or from public or private research centers.

L'archive ouverte pluridisciplinaire **HAL**, est destinée au dépôt et à la diffusion de documents scientifiques de niveau recherche, publiés ou non, émanant des établissements d'enseignement et de recherche français ou étrangers, des laboratoires publics ou privés.

A detailed experimental and kinetic modeling study on pyrolysis and oxidation of oxymethylene ether-2 (OME-2)

Kevin De Ras^a, Marvin Kusenberga, Guillaume Vanhove^b, Yann Fenard^b, Andreas Eschenbacher^a, Robin J. Varghese^a, Jeroen Aerssens^a, Ruben Van de Vijver^a, Luc-Sy Tran^b, Joris W. Thybaut^a, Kevin M. Van Geem^{a,*}

^a Laboratory for Chemical Technology (LCT), Ghent University, Technologiepark 125, B-9052 Ghent, Belgium

^b PhysicoChimie des Processus de Combustion et de l'Atmosphère (PC2A) - UMR 8522, University of Lille, CNRS, F-59000 Lille, France

Abstract:

The application of oxymethylene ethers as an alternative fuel (additive) produced via carbon capture and utilization can lead to lower CO₂ and particulate matter emissions compared to fossil fuels. To improve the understanding of the pyrolysis and oxidation chemistry of oxymethylene ether-2 (OME-2), a combined experimental and kinetic modeling study has been carried out. Pyrolysis experiments were performed using a quartz reactor over a broad temperature range, from 373 to 1150 K, to elucidate both the primary and secondary pyrolysis chemistry. The thermal decomposition of OME-2 is initiated via a dominant formaldehyde elimination reaction. Radical chemistry becomes only significant at higher temperatures (>800 K) and competes with unimolecular decomposition. Radicals originate mainly from the decomposition of carbenes. Important intermediate products formed during pyrolysis are dimethoxymethane, formaldehyde, methane and methyl formate. The formation of products with carbon-carbon bonds is minor since only carbon-oxygen bonds are present in OME-2. The oxidation chemistry was investigated between 600 and 715 K by ignition delay time measurements in a rapid compression machine for OME-2/air mixtures with an equivalence ratio ϕ of 0.5. No negative temperature coefficient region is observed. An elementary step kinetic model is constructed with the automatic kinetic model generator Genesys starting from the base mechanism AramcoMech 1.3. Important thermodynamic parameters and reaction rate coefficients to describe the low- and high-temperature decomposition chemistry are obtained from quantum chemical calculations. The new kinetic model satisfactorily reproduces the measured ignition delay times, as well as major product mole fractions from the pyrolysis experiments within the experimental error margin of 10 % on average, without fitting thermodynamic or kinetic parameters. Finally, rate of production analyses reveal the important decomposition pathways to methyl formate, formaldehyde and others under pyrolysis and low-temperature oxidation conditions.

Keywords: Polyoxymethylene dimethyl ethers, Oxymethylene ether-2, Quantum chemistry, Automatic kinetic modeling, Pyrolysis, Oxidation.

1. Introduction

The need to reduce greenhouse gas and pollutant emissions to combat environmental issues and the desire for a circular carbon economy to create a sustainable society have encouraged researchers to unravel the field of novel renewable fuels and fuel additives. Oxymethylene ethers (OMEs), more formally known as polyoxymethylene dimethyl ethers (PODEs), represent a family of molecules with alternating carbon and oxygen atoms in the backbone saturated with hydrogen, corresponding with the structural formula $\text{CH}_3\text{O}(\text{CH}_2\text{O})_n\text{CH}_3$ (OME- n). These molecules form a high-potential class of sustainable synthetic fuels when produced via carbon capture and utilization, i.e., starting from captured CO and CO₂, and renewable electricity [1-3]. Several engine studies have already demonstrated the advantageous combustion characteristics of pure OMEs and OME-diesel blends over conventional diesel, resulting in cleaner exhaust gases [4-11]. However, understanding the pyrolysis and combustion chemistry remains a prerequisite to introducing OMEs as fuel (additive) on a large scale. The present work is the first detailed study focusing on both the pyrolysis and oxidation of OME-2 (synonyms are PODE-2, methoxy(methoxymethoxy)methane and 2,4,6-trioxaheptane). Despite OME-2 not being directly eligible for fuel applications due to its low flash and boiling point [8, 9], the obtained chemical insight from this small, model OME is essential to develop detailed kinetic models for larger OMEs in the future.

The pyrolysis and oxidation of dimethoxymethane (DMM), sometimes referred to as methylal or OME-1, has already been investigated extensively before by both experimental and kinetic modeling studies [12-16]. Several of these studies report DMM-specific thermodynamic parameters and reaction rate coefficients obtained from quantum chemical calculations [12, 14]. A combined experimental and kinetic modeling study was recently published on the oxidation of methoxymethanol for which high-level quantum chemical calculations were carried out for hydrogen abstractions by Zhu et al. [17, 18]. The experimental data were obtained from methanol/formaldehyde mixtures which are in equilibrium with methoxymethanol. The available literature on modeling the oxidation of longer chain OMEs is limited, i.e., work performed by Cai et al. (OME-2/3/4) [19], He et al. (OME-3) [20], Sun et al. (OME-3) [21] and Zhao et al. (OME-3) [22]. These models rely on extrapolation of thermodynamic parameters and reaction rate coefficients from dimethyl ether (DME) and DMM, as pointed out in a review study by Fenard et al. [23]. However, detailed quantum chemical studies do not exist for larger OMEs. The only available experimental data related to the oxidation of OME-2 are measured ignition delay times. Cai et al. [19] investigated the auto-ignition of OME-2/air mixtures in a shock tube for a range of equivalence ratios (ϕ equal to 0.5, 1.0 and 2.5) at 0.20 MPa and for a stoichiometric mixture at 0.10 MPa. Drost et al. [24] performed experiments with a stoichiometric OME-2/air mixture in a rapid compression machine for pressures ranging from 0.4 to 1.0 MPa and temperatures between 560 and 839 K. Detailed kinetic models for the pyrolysis of OMEs and associated experimental data are not yet available in the literature.

In this work, both the pyrolysis and the low-temperature oxidation chemistry of OME-2 are studied experimentally and theoretically through simulations with a newly developed kinetic model. Pyrolysis experiments have been performed using a tubular quartz reactor at 0.34 MPa. The experiments cover a broad temperature range to validate both the primary and

secondary chemistry of the reaction mechanism. For the low-temperature oxidation, ignition delay times have been measured during rapid compression machine experiments for an equivalence ratio ϕ of 0.5 at pressures of 0.5 and 1.0 MPa. The in-house developed automatic kinetic model generator Genesys [25] is used to construct an elementary step kinetic model for the pyrolysis and oxidation of OME-2 based on the reaction families from DMM [12]. The developed model includes quantum chemically calculated thermodynamic and kinetic parameters for important species and reactions, respectively. Rate of production and sensitivity analyses are carried out for pyrolysis and oxidation to investigate the dominant reaction pathways under varying reaction conditions.

2. Experimental methods

Experimental data are acquired from two different experimental units, both using as reactant OME-2 (purity > 98.5 mol%, with the main impurities DMM \pm 1.0 mol% and OME-3 \pm 0.3 mol%, as confirmed by two-dimensional gas chromatography analysis) supplied by ASG Analytik-Service GmbH, Germany.

2.1. Pyrolysis in a micro-pyrolysis unit

A micro-pyrolysis unit [26] consisting of two main sections, i.e., the reactor and on-line product analysis section, is used to evaluate the pyrolysis chemistry at low and high temperatures. The reactor section is a tandem micropyrolyzer (Rx-3050TR Frontier Labs, Japan) consisting of two quartz reactor tubes in series accurately maintained at isothermal conditions. The analysis section comprises a two-dimensional gas chromatography (GC \times GC, Thermo Scientific TRACE Ultra) coupled to flame ionization detection (FID) and time-of-flight mass spectroscopy (ToF-MS), as well as a dedicated multicolumn GC (Thermo Scientific Trace 1310), termed the light oxygenates analyzer (LOA), equipped with thermal conductivity (TCD) and pulsed discharge (PDD) detectors. The ToF-MS is used for identification of detected compounds in the reactor effluent. These reaction products were manually identified based on the measured mass spectra and the possible fractionation pathways of species in molecular fragments via interaction with highly energized electrons. In particular, identification of DME, DMM, OME-2 and methyl formate were confirmed via injection of the pure products. The LOA is used to analyze light gases (H_2 , CO, CO_2 , CH_4), H_2O , and small oxygenates such as CH_2O . GC \times GC – FID analysis is used to quantify larger oxygenated compounds, including DME, DMM and OME-2. A two-stage liquid CO_2 modulator is placed at the end of the first dimension column in the GC \times GC. The first column separates products based on their volatility, while the second column separates compounds based on their polarity. The characteristics and settings of the on-line GC \times GC – FID/MS analyses are provided in the **Supplementary Information**. More detailed information about the GC \times GC, multicolumn GC and the micro-pyrolysis unit is reported in previous work [26, 27].

For the present work, the temperature of the first reactor is continuously held at 423 K. Multiple measurements are performed for the different temperature conditions of the second reactor, with 0.3 μ L of OME-2 being introduced into the first reactor via a septum using a 0.5 μ L syringe. Upon manual injection in this heated zone, the drop that formed at the tip of

the injected needle evaporates, and the vapors are transported into the second reactor with the He carrier gas (Air Products, Belgium, purity 99.999 mol%) at a flow rate of 82 Nml min⁻¹. An additional 10 Nml min⁻¹ of He gas is added at the interface between the first and second reactor. The distribution of the OME-2 vapor pulse leaving the second reactor under non-reactive conditions has been determined, with details of the measurements and results provided in the **Supplementary Information**. The actual thermal decomposition proceeds in the second reactor, which is investigated in the temperature range 373 to 1073 K at a pressure of 0.34 MPa. This tubular quartz reactor has a length of 120 mm and an inner diameter of 4.0 mm with a wall thickness of 2.0 mm. The pressure drop over the reactor is negligible. The temperature profiles in the second reactor have been measured under non-reactive conditions using an N-type thermocouple and are provided in the **Supplementary Information**. A micro-jet cryotrap located inside the GC × GC held the reactor effluent for 5 minutes inside a guard column section by cooling with liquid N₂ at 88 K. Once the liquid N₂ cooling was switched off, the trapped vapors are immediately heated to the oven temperature (313 K), and the desorbed and refocused product vapors are then split into two streams for simultaneous analysis by GC × GC - FID and the GC - LOA (split ratio 50:1 at GC inlet).

Elemental balances are closed within 100 ± 5 % for all experimental conditions. Product yields and associated uncertainties are provided in the **Supplementary Information**.

2.2. Ignition delay time measurements in a rapid compression machine

The ULille Rapid Compression Machine (RCM) has been used to measure first-stage (FSIDT) and total ignition delay times (IDT) of OME-2/air mixtures. This RCM is pneumatically driven and uses a right-angle design to eliminate the risk of rebound at Top Dead Center (TDC) and to maximize the reproducibility of the compression phase. Only the details relevant to this study are given here since this device has been described extensively in previous studies [28-30]. Mixtures containing OME-2, molecular oxygen and inert gases are prepared using a mixture preparation facility, with an equivalence ratio ϕ of 0.5, relevant to the use of OME-2 in modern compression ignition applications. N₂, CO₂ and Ar are used as inert gases. The purities of the pure gases, as obtained from Air Liquide France, are above 99.99 mol%. The liquid fuel has been further purified from eventually dissolved gases by several freeze-pump distillation cycles.

The prepared “air” mixtures, with an inert-to-O₂ ratio of 4, are compressed at 0.5 MPa and 1.0 MPa inside the RCM with a compression time of about 45 ms, and a creviced piston head dedicated to prevent the formation of a piston corner vortex after compression. The pressure is measured by two (6052 and 601CA) thermal shock-protected piezoelectric Kistler pressure transducers, the signal being recorded with a 40 μs timestep. The compressed temperature (T_C) is calculated using the adiabatic core gas hypothesis from the initial pressure, temperature and compressed pressure (P_C). An uncertainty of ± 5 K is assumed on T_C. All ignition delay experiments are repeated at least three times per condition to show reproducibility in the experimental data. The FSIDT and IDT are defined as the elapsed time between the end of the compression and the moment where the pressure rise rate is at its maximum value caused by first- and second-stage auto-ignition, respectively, as depicted in

Fig. 1. The volume histories have been obtained from non-reactive experiments where the molecular oxygen fraction was replaced by N₂.

The experimental results, as well as the measured volume histories, are available in the **Supplementary Information**.

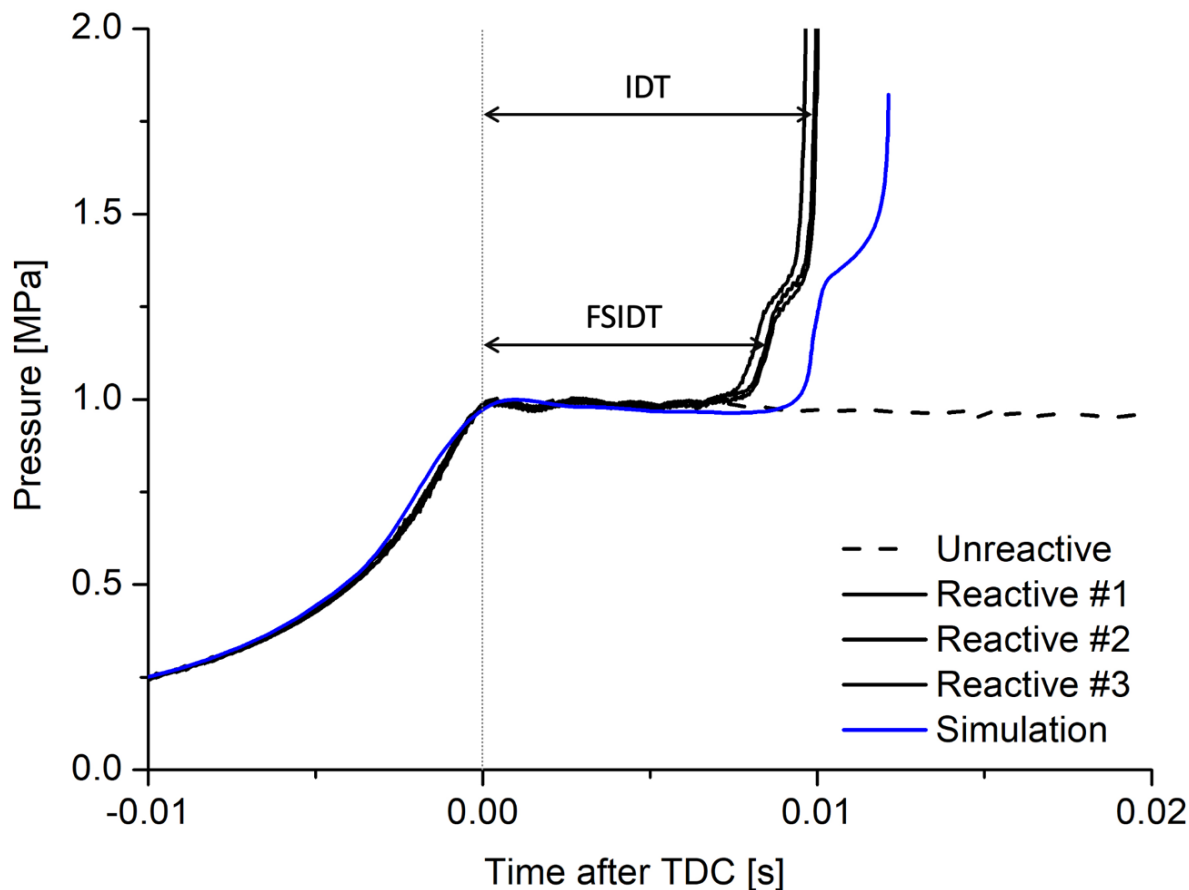


Fig. 1. Non-reactive and reactive experimental pressure profiles obtained from the ULille RCM and simulation results with the developed kinetic model with indication of the first-stage ignition delay time (FSIDT) and total ignition delay time (IDT). The pressure profiles are for a mixture of 1.96 mol% OME-2, 19.61 mol% O₂ and 78.43 mol% N₂ ($\phi = 0.5$) at a T_c of 663 ± 5 K and P_c of 1.0 ± 0.03 MPa.

3. Computational methods

Quantum chemical calculations are performed on the high-performance computing infrastructure of Ghent University at the CBS-QB3 level of theory as implemented in Gaussian 16 [31]. The lowest energy conformer is extensively searched by optimizing most likely structures at the CBS-QB3 level of theory combined with performing 1-dimensional rotational scans around each internal bond. In the case of multiple possible stereoisomers for a molecule, only the one corresponding with the lowest electronic energy is retained. The thermodynamic parameters, i.e., the standard enthalpy of formation, the standard intrinsic

entropy and specific heat capacities at different temperatures, are calculated for both species and transition states from the CBS-QB3 results by applying principles of ideal gas statistical thermodynamics. Internal modes are treated as harmonic oscillators except for modes that resemble rotations around single bonds. The latter are approximated by 1-dimensional hindered internal rotations (1D-HIR) as long as the electronic barrier does not exceed 100 kJ mol⁻¹. The hindrance potentials are calculated at the B3LYP/6-31G(d) level of theory with (semi-)relaxed surface scans in which all coordinates, except for the dihedral angle of interest, are re-optimized at each scan angle with a step size of 10°. To obtain smooth surface scans corresponding with the rotation of the bond of interest, it is sometimes necessary to fix adjacent bond lengths, bond angles and/or dihedral angles. The Fourier series expression of the hindrance potential together with the reduced moment of inertia calculated at the I^(2,3) level, as defined by East and Radom [32], are used to construct the Schrödinger equation for 1-dimensional internal rotation. The eigenvalues of the solution are used to determine the partition function as a function of temperature. Thermodynamic parameters are calculated from the total partition function taking into account the symmetry and the number of optical isomers (enantiomers). The atomization method is used to calculate the enthalpy of formation. Two corrections are applied to correct the enthalpy of formation calculated at the CBS-QB3 level of theory for systematic errors, i.e., spin-orbit corrections (SOC) [33] as these are not part of the CBS-QB3 methodology and empirical bond additive corrections (BAC) [34, 35]. There is no SOC and BAC contribution applied in case only relative enthalpies are required, i.e., for the calculation of reaction rate coefficients and the construction of potential energy surfaces. NASA polynomials are regressed from the thermodynamic parameters, which are valid in a temperature range from 300 to 3000 K. Conventional transition state theory is used to calculate the high-pressure limit reaction rate coefficients over a temperature range of 300 to 2000 K, with the asymmetric Eckart potential to account for tunneling [36]. Modified Arrhenius parameters (A , n , E_a), as defined in **Eq. (1)**, are obtained by linear regression of rate coefficients over the same temperature range. In this equation, $k(T)$ is the reaction rate coefficient, T the absolute temperature and R the universal gas constant.

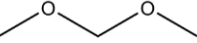


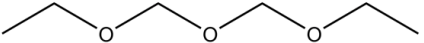
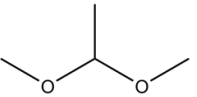
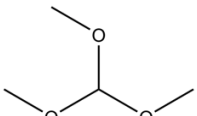
$$k(T) = A \cdot \left(\frac{T}{1\text{ K}}\right)^n \cdot \exp\left(-\frac{E_a}{RT}\right) \quad (1)$$

Based on the work of Paraskevas et al. [37], it is assumed that with the described approach, the enthalpies of formation at 298 K are calculated within 4 kJ mol⁻¹ (chemical accuracy) for non-radical compounds. The entropies at 298 K and specific heat capacities at multiple temperatures are similarly expected to be reproduced within 4 J mol⁻¹ K⁻¹. These accuracies were obtained by comparing thermodynamic parameters determined at the CBS-QB3 level of theory with experimental data for oxygenates. Validation of thermodynamic parameters for OME-2 or derivatives is not possible due to the absence of experimental data. In **Table 1**, the enthalpy of formation calculated for several compounds with similar functionalities is compared with experimental values from the National Institute of Standards and Technology (NIST) WebBook [38], all in agreement with the presumed accuracy. Similarly, multiple studies have been performed to assess the accuracy of reaction rate coefficients calculated at the CBS-QB3 level of theory, including the 1D-HIR correction and Eckart tunneling [39-41]. With this approach, the uncertainty of the reaction rate coefficients is assumed to be

within a factor 2 - 4. Note that the larger factor of 4 accounts for uncertainties in entropy values caused by the coupling of internal rotors due to hydrogen bonds.

A complete list of the thermodynamic and kinetic parameters calculated for the kinetic model at the CBS-QB3 level of theory is provided in the **Supplementary Information**. Geometries for species and transition states presented in this work are provided as well.

Table 1. Comparison between experimental and quantum chemical calculated enthalpies of formation at 298 K ($\Delta H_f^{298 K}$). The experimental data is provided with the reported uncertainty.

| Molecule | NIST [kJ mol ⁻¹] | This study [kJ mol ⁻¹] |
|---|------------------------------|------------------------------------|
|  | -348.2 ± 0.8 | -351.4 |
|  | -342.8 ± 0.7 | -342.5 |
|  | -408.2 ± 1.0 | -409.8 |
|  | -581.1 ± 1.1 | -580.4 |
|  | -389.7 ± 0.8 | -390.9 |
|  | -531.8 ± 3.2 | -532.2 |

4. Kinetic model development

A first principles-based kinetic model for pyrolysis and oxidation of OME-2 is constructed using the automatic kinetic model generation tool Genesys [25]. A number of initial species, a set of user-defined reaction families and associated constraints are specified as input for Genesys to generate the reaction network. Reaction families specify the molecular rearrangements to go from reactant(s) to product(s) by means of an elementary reaction [42]. The used reaction families for this study are based on earlier work for DMM with Genesys [12]. Thermodynamic consistency within the model, i.e., fulfilling the fundamental relation between the forward and reverse reaction rate coefficients and the equilibrium coefficient, is ensured by defining the reactions as reversible. Reactions forming three or more products are an exception for which only the forward reaction is defined since the reverse reaction involving the simultaneous collision of three or more molecules with correct orientation will rarely occur. To prevent unlimited extension of the reaction mechanism, resulting in the inclusion of kinetically insignificant species and reactions, a rule-based termination criterion is applied. The rules or constraints are specified on the level of reaction families and generated product species. The Genesys model does not include reactions between species with carbon-carbon

bonds and OMEs. Furthermore, the addition of hydroperoxy alkyl radicals to molecular oxygen is not included in the generated reaction network. This would require additional computational expensive calculations, which are redundant to simulate the performed experiments.

After generating the complete OME-2 reaction network, thermodynamic and kinetic parameters are assigned to all species and reactions respectively. For this, Genesys makes use of user-defined databases containing thermodynamic and kinetic data obtained from quantum chemical calculations. Such calculations are performed for species and reactions related to pathways believed to be important during pyrolysis and oxidation of OME-2. When there are no quantum chemical data available, thermodynamic parameters are calculated using Benson's group additivity method. A new group additivity scheme is developed with the available OME thermodynamic data set because an assessment of the default scheme indicated bad performance for OMEs and derived compounds. Given that quantum chemical kinetic data would be missing for a reaction, the kinetic group additivity method developed by Saeys et al. [43], rate rules or analogies of similar reactions are used to assign (modified) Arrhenius parameters. In the case of pyrolysis, the most important reaction families are the hydrogen abstractions, hydrogen shifts and β -scissions for which in-house developed rate rules were developed specifically for OMEs to overcome a lack of kinetic data and avoid using alkane analogies. For several hydrogen abstractions by the hydroxyl radical, an analogy is used from the study on methoxymethanol [17, 18] for which high-level quantum chemical calculations were performed. The kinetic group additive values for oxygenates determined by Paraskevas et al. [44] are used for the remaining hydrogen abstractions. Modified Arrhenius parameters for the low-temperature oxidation reactions are assigned via reactivity-structure-based rate rules determined by Cai et al. [45] and Bugler et al. [46] when no quantum chemical data is available.

The generated kinetic model for OME-2 from Genesys is finally merged with a base mechanism, i.e., AramcoMech 1.3 [47]. The latter mechanism contains 124 species and 766 reactions and describes the oxidation chemistry of C₁-C₄ based hydrocarbons and oxygenated compounds including DME. All species containing carbon-carbon bonds appear in the kinetic model through this merge. In the case of conflicting thermodynamic or kinetic parameters, the input of the AramcoMech model is retained to maintain the integrity of this experimentally fitted model. The AramcoMech 1.3 mechanism is chosen over more recently extended versions based on the experience of earlier studies by the authors [12, 48]. The complete kinetic model for pyrolysis and oxidation, consisting of 301 species and 2251 reactions, is available in the **Supplementary Information** in CHEMKIN format.

5. Results and discussion

In analogy with alkanes, a carbon atom connected to 3 hydrogen atoms and 1 oxygen atom is designated as a primary carbon atom, a carbon atom connected to 2 hydrogen atoms and 2 oxygen atoms as a secondary carbon atom, and a carbon atom connected to 1 hydrogen atom and 3 oxygen atoms as a tertiary carbon atom. The same notation holds for the associated radicals.

5.1. Initiation reaction pathways

The decomposition of OME-2 during pyrolysis and oxidation is driven by free radical chemistry. In the case of pyrolysis, the formation of radicals originates from homolytic bond scissions. During oxidation, radicals are initially formed via hydrogen abstraction by molecular oxygen. The bond dissociation energies (BDE) of OME-2 at 0 K are depicted in **Fig. 2**, also indicating the nomenclature used in this work. The BDEs of DME and DMM are similarly indicated for comparison. For the lowest energy conformer, the backbone of the OME-2 molecule forms a helix-like structure with dihedral angles ranging between 68 and 75°, indicating that multiple consecutive methylene-oxygen repeat units favor gauche interactions.

The outer carbon-oxygen bond, i.e., the C₁-O₁ bond, is the weakest in OME-2, with a BDE amounting to 348.3 kJ mol⁻¹. This corresponds well with the BDE of C-O bonds from an ether functional group (e.g., in DME) and with the BDE of C₁-O in DMM. The other C-O bonds in OME-2 are significantly stronger (> 20 kJ mol⁻¹) and have similar dissociation energies, 376.9 and 373.2 kJ mol⁻¹ for C₂-O₁ and C₂-O₂, respectively, as can be expected due to their identical chemical moiety. These values are similar to the dissociation energy of C₂-O in DMM, i.e., 374.4 kJ mol⁻¹. The BDEs of the C₁-H and C₂-H bonds in OME-2 are equal to 403.9 and 404.5 kJ mol⁻¹, respectively. Consecutive C-O bonds clearly reduce the BDE of nearby C-H bonds in OMEs compared to alkane analogues. The BDE of a primary and secondary C-H bond in an alkane amounts to approximately 423 and 411 kJ mol⁻¹, respectively. The calculated enthalpy of formation at 298 K for C[•]OCOCOC (labeled as R₁[•]) amounts to -322.8 kJ mol⁻¹ and equals -321.8 kJ mol⁻¹ for COC[•]OCOC (labeled as R₂[•]), approximately the same value, even though one is a primary and the other a secondary radical. Two effects have to be considered for this radical stability. First, each neighbor oxygen atom of a carbon radical provides stabilization due to electron delocalization. Second, sp²-hybridization disturbs the energetic favorable gauche interactions in secondary radicals.

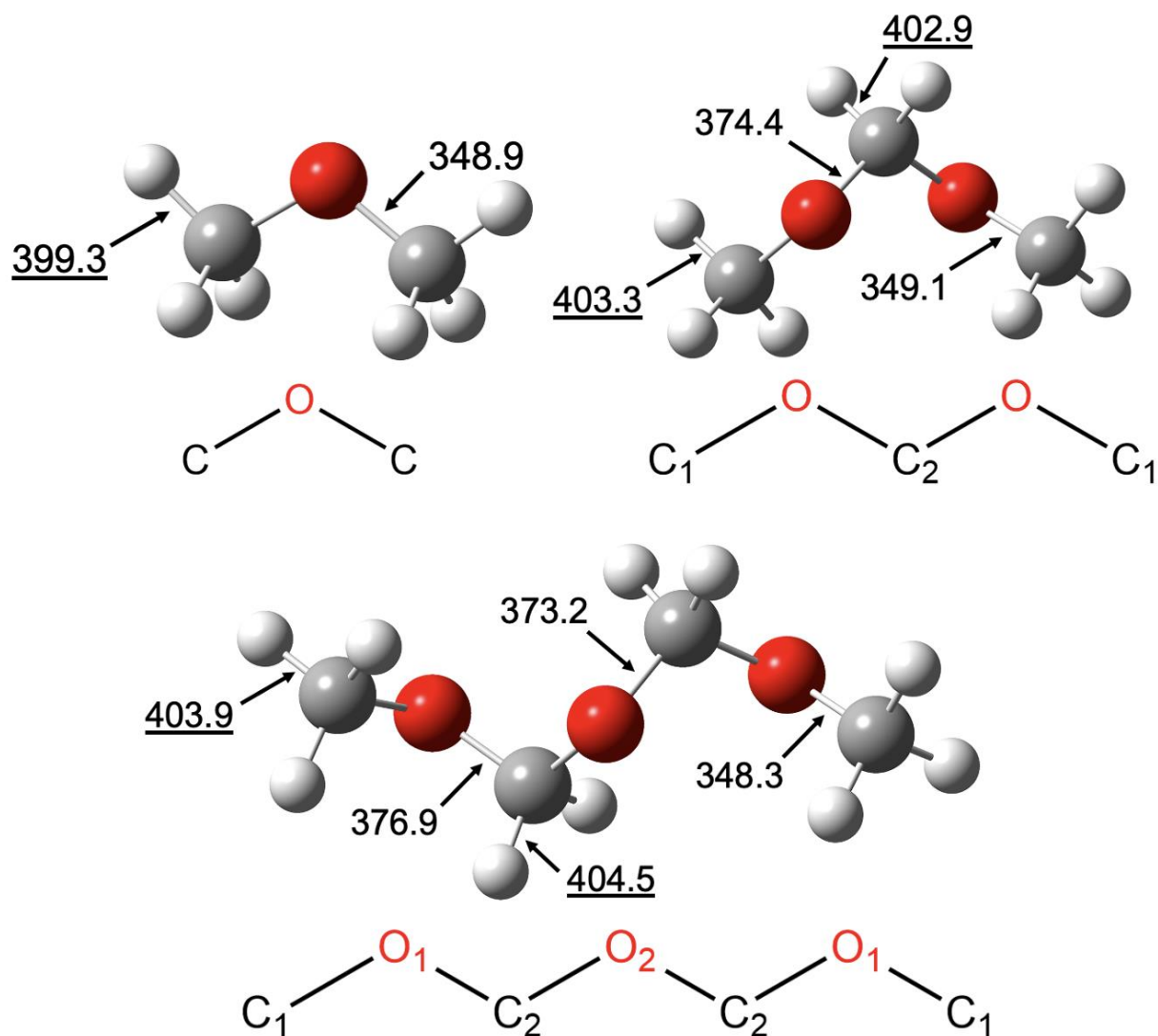


Fig. 2. Bond dissociation energies (BDE) at 0 K, in kJ mol⁻¹, for dimethyl ether (top left), dimethoxymethane (top right) and oxymethylene ether-2 (bottom) at the CBS-QB3 level of theory. The BDE of carbon-hydrogen bonds is underlined for clarity. The skeletal formula indicates the nomenclature used for atoms in this work.


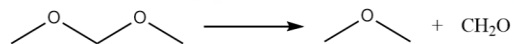
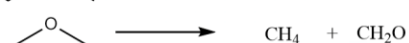
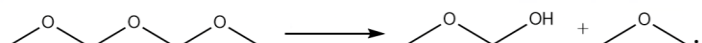
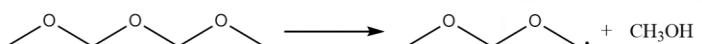


In addition to the typical pyrolysis and oxidation radical reactions, several other unimolecular decomposition pathways are possible for OMEs. These unimolecular reactions are searched via quantum chemical calculations and depicted by means of potential energy surfaces for DME, DMM and OME-2 in **Fig. 3**. All transition states have been verified by performing intrinsic reaction coordinate calculations. The lowest BDE in the molecule is represented by the red line, i.e., an indication of the electronic energy required for the barrierless homolytic scission reaction. For OME-2, it represents the scission creating the methyl and methoxymethoxymethoxy radical (COCOCO[•]). Several reaction pathways are

available with significantly lower electronic barriers which are therefore more likely to proceed. In the case of DME, decomposition forming methane and formaldehyde is favored via a tight transition state with an electronic barrier of only 307.0 kJ mol⁻¹ compared to 348.9 kJ mol⁻¹, i.e., the BDE of the C-O bond. The roaming reaction forming methanol and methylene proceeds via a higher activated transition state of 356.4 kJ mol⁻¹. All roaming reactions producing methylene form a van der Waals-complex with the associated alcohol. The situation becomes more complex for longer molecules. In the case of OME-2, there are three possible transition states for an endothermic formaldehyde elimination reaction, one for each C-O bond, which can serve as the origin for formaldehyde. The lowest electronic barrier amounts to 276.1 kJ mol⁻¹ corresponding with the elimination of a C₂-O₂ bond and the barriers of 326.7 and 360.6 kJ mol⁻¹ correspond with the elimination of C₂-O₁ and C₁-O₁, respectively. Two other exothermic reactions form very stable species, i.e., methane and methoxymethyl formate or DME and methyl formate, but with too high electronic barriers to play an important role. All these concerted reactions have as a common feature the breaking of two single bonds, i.e., two C-O bonds or a C-O and C-H bond, and the formation of one carbonyl functionality. This is different for the highly endothermic roaming reactions where a C-H and C-O bond is broken with the formation of a hydroxyl functionality. The second-lowest electronic barrier for OME-2 amounts to 282.1 kJ mol⁻¹ for the roaming reaction forming methoxycarbene and methoxymethanol. Methoxycarbene is unstable and can quickly decompose by an activated homolytic scission reaction forming the methyl and formyl radicals. Once radicals appear in the reaction system, these can initiate the radical chemistry of OME-2 by bimolecular hydrogen abstraction reactions. The other roaming reaction with an electronic barrier of 299.9 kJ mol⁻¹ forming the methoxymethoxycarbene and methanol is less important but will also generate radicals via decomposition of the carbene into the methoxymethyl and formyl radical. Once sufficient amounts of radicals exist in the reaction environment, these will significantly affect the reactivity since electronic barriers of radical chemistry reactions are far below the aforementioned barriers.

Similar results are obtained for unimolecular decomposition of DMM (cf. **Fig. 3**), except that a low barrier formaldehyde elimination reaction does not exist. The roaming reaction with the formation of methoxycarbene and methanol is the most favorable reaction pathway with an electronic barrier of 299.4 kJ mol⁻¹. In **Table 2**, modified Arrhenius parameters associated with the important unimolecular decomposition pathways of DME, DMM and OME-2 are listed as obtained from the quantum chemical calculations. For the formaldehyde eliminations, only the parameters associated with the lowest transition state are listed. A study by Döntgen et al. [49] reported Arrhenius parameters for the alkoxy roaming reactions of DMM and OME-2, forming methanol and the associated carbene. Their reported reaction rate coefficients are on average one order of magnitude smaller compared with our calculated rate coefficients. This deviation can be devoted to the different levels of theory used, the inclusion of quantum chemical tunneling in our study and the choice to report a constant pre-exponential factor for all roaming reactions in the mentioned study.

Table 2. Modified Arrhenius parameters obtained from quantum chemical calculations at the CBS-QB3 level of theory for the important unimolecular decomposition pathways regressed

from the high-pressure limit reaction rate coefficients in the temperature range 300 to 2000 K.

| Reaction | A [s ⁻¹] | n [-] | E _a [kJ mol ⁻¹] |
|---|-------------------------|----------|---|
|  | ¹ 2.33 E+15 | 0.31 | 270.8 |
|  | ¹ 9.54 E+14 | 0.39 | 308.9 |
|  | 6.73 E+03 | 3.53 | 283.8 |
|  | 3.08 E+14 | 0.88 | 308.2 |
|  | 2.83 E+13 | 0.57 | 298.0 |
|  | 3.34 E+13 | 0.53 | 294.5 |
|  | 1.33 E+11 | 1.05 | 172.4 |

¹ Values correspond with the lowest activated transition state - the reaction rate coefficient for the other transition state(s) is several orders of magnitude smaller.

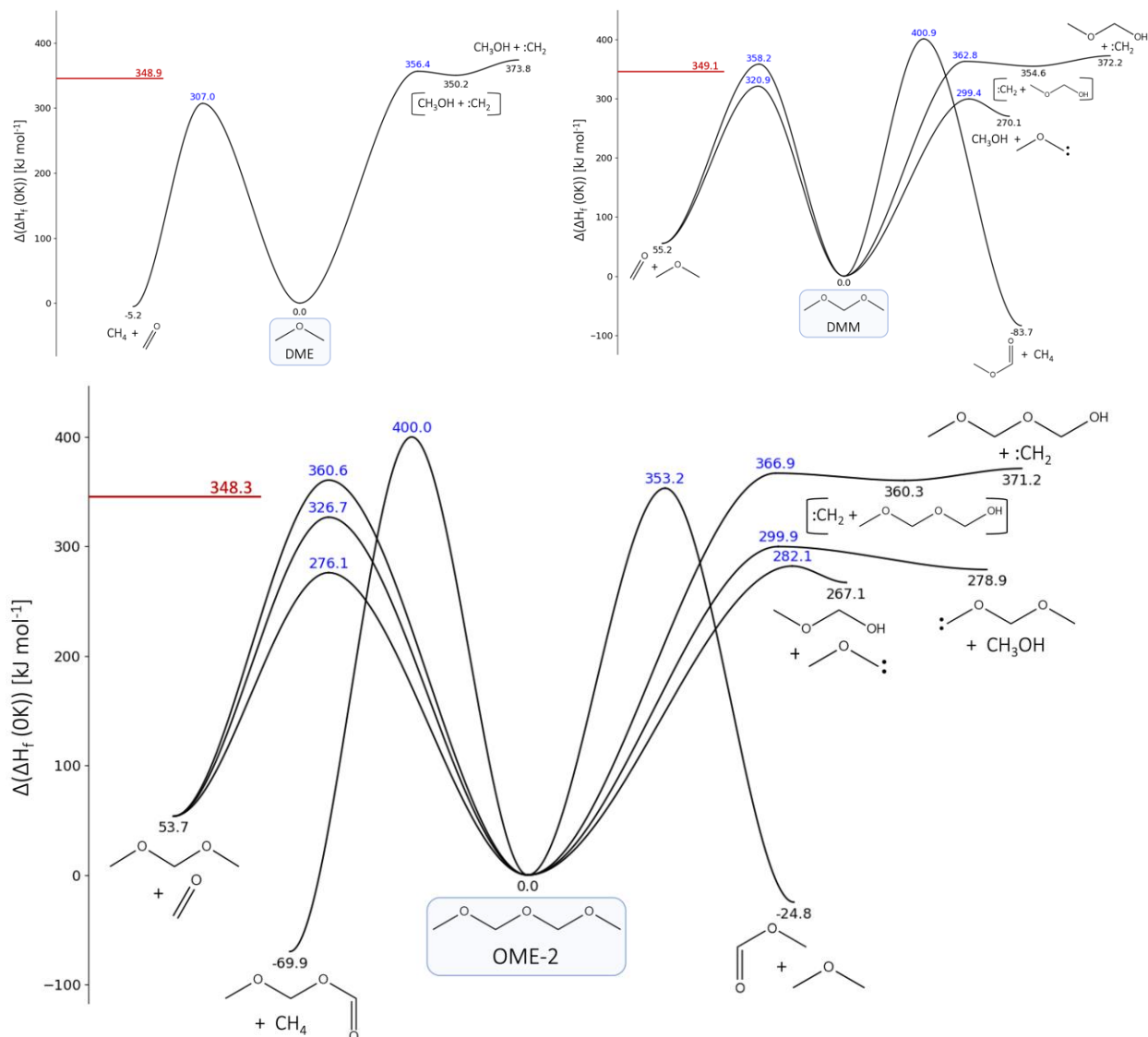


Fig. 3. Schematic potential energy surfaces for unimolecular decomposition of dimethyl ether (top left), dimethoxymethane (top right) and oxymethylene ether-2 (bottom) by non-homolytic scission reactions. The values are CBS-QB3 calculated enthalpies of formation at 0 K relative to the enthalpy of formation of the respective molecule (DME, DMM or OME-2). The red line indicates the lowest BDE of each molecule. Products between brackets indicate the formation of a van der Waals-well.

The lowest electronic barriers for hydrogen abstraction by molecular oxygen from the primary and secondary carbon atom in OME-2 amount to 179.4 and 169.5 kJ mol^{-1} , respectively. In both cases, the OME-2 radical and the hydroperoxyl radical form a van der Waals well which requires an additional amount of energy to form the different products as depicted in **Fig. 4**. Though, the electronic barriers are significantly lower than barriers of the

aforementioned unimolecular reaction pathways, decomposition of OME-2 by oxidation will therefore start at remarkably lower temperatures than pyrolysis.

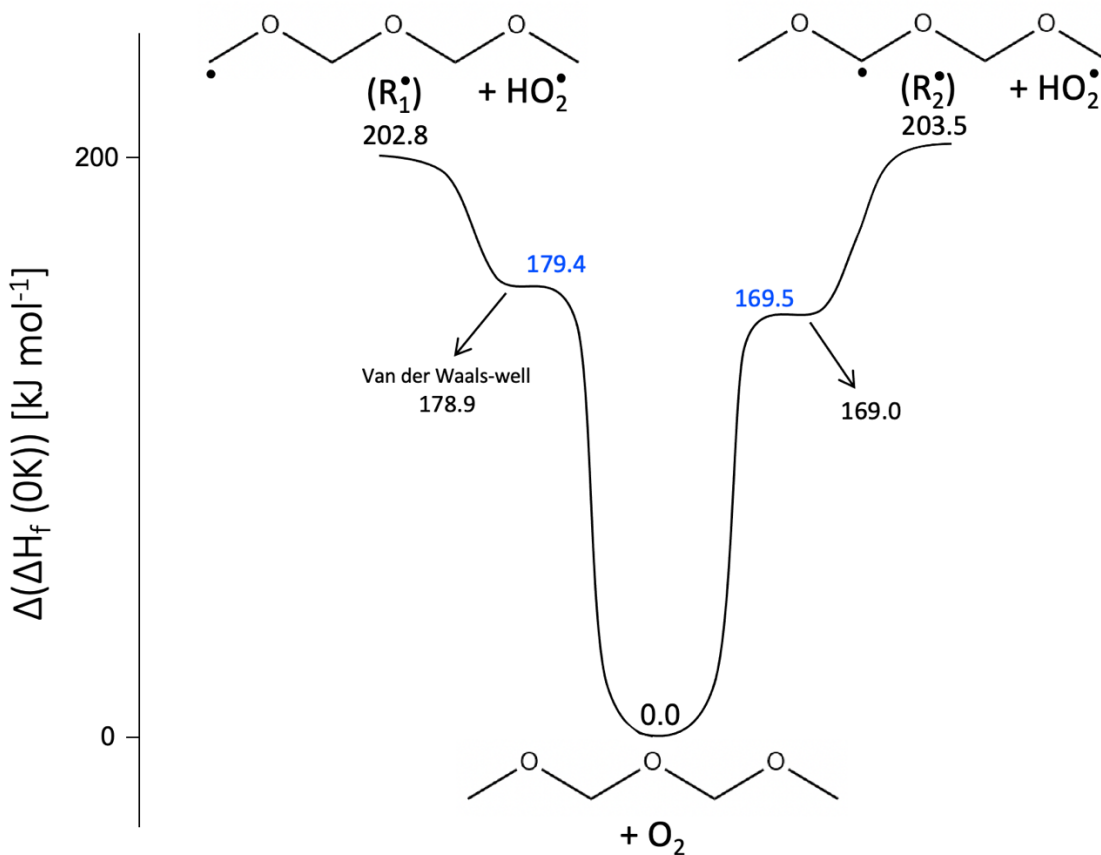


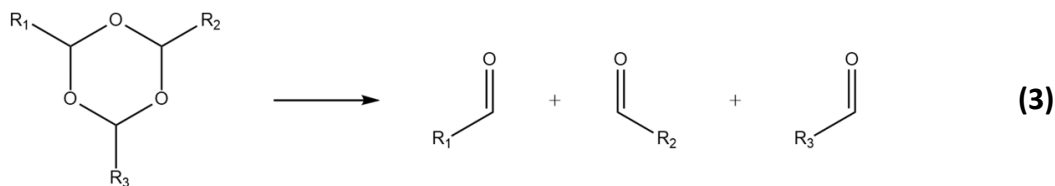
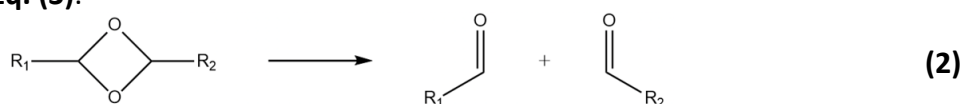
Fig. 4. Schematic potential energy surface for the hydrogen abstraction from OME-2 by molecular oxygen. The values are CBS-QB3 calculated enthalpies of formation at 0 K relative to the sum of the enthalpy of formation of OME-2 and molecular oxygen (triplet spin multiplicity).

5.2. Potential energy surfaces for low-temperature oxidation

Two peroxy radicals (ROO^\bullet) can be formed by the barrierless addition of an OME-2 carbon-centered radical, i.e., R_1^\bullet and R_2^\bullet , to molecular oxygen. The addition of R_1^\bullet to O_2 and R_2^\bullet to O_2 corresponds to an electronic reaction enthalpy of -145.7 and -158.7 kJ mol^{-1} , respectively. For comparison, the CBS-QB3 calculated C-OO $^\bullet$ BDE in the ethylperoxy radical amounts to 142.6 kJ mol^{-1} and 151.3 kJ mol^{-1} for the isopropylperoxy radical. The influence of radical addition to O_2 during low-temperature oxidation of OME-2 is investigated by constructing the potential energy surfaces as depicted in **Fig. 5** for $\text{R}_2\text{OO}^\bullet$. The latter is expected to play a more dominant role than $\text{R}_1\text{OO}^\bullet$ due to the easier formation via hydrogen abstraction by molecular oxygen.

Only elementary reactions for which the relative energy of the transition state remains below the reaction enthalpy of the dissociation of molecular oxygen are considered.

The formed peroxide radical R_2OO^\bullet can react via several reaction pathways, amongst which isomerization by an intramolecular hydrogen abstraction or hydroxyl-shift, cyclic ether formation, β -scission, etc. First, an intramolecular hydrogen abstraction in R_2OO^\bullet accompanied by a molecular rearrangement leads to methoxymethyl methyl carbonate and the hydroxyl radical. This reaction is highly exothermic, i.e., a reaction enthalpy amounting to $-207.1 \text{ kJ mol}^{-1}$, but involves a tight four-membered cyclic transition state with an electronic barrier of $156.3 \text{ kJ mol}^{-1}$. More favorable pathways are the intramolecular hydrogen abstractions forming Q_1OOH ($C^\bullet OC(OOH)OCOC$), Q_2OOH ($COC(OOH)OC^\bullet OC$) or Q_3OOH ($COC(OOH)OCOC^\bullet$) via a six-, six- and eight-membered cyclic transition state, respectively. The electronic barrier for the formation of Q_2OOH is the lowest amounting to 76.7 kJ mol^{-1} , compared to 89.4 kJ mol^{-1} for Q_1OOH and 83.2 kJ mol^{-1} for Q_3OOH . The stabilities of the formed primary and secondary hydroperoxy alkyl radicals are very similar, all having intramolecular hydrogen bonds. Q_2OOH can subsequently react via β -scission of the C_1-O_1 bond or the C_2-O_2 bond with barriers of 72.3 and 59.1 kJ mol^{-1} , respectively. In the case of the C_2-O_2 bond, the $COC^\bullet OOH$ structure undergoes a simultaneous molecular rearrangement to form methyl formate and the hydroxyl radical. The formation of 1,3-dimethoxy-1,3-dioxetane and the hydroxyl radical from Q_2OOH has the lowest electronic barrier, i.e., only 48.1 kJ mol^{-1} . Similarly, for Q_1OOH and Q_3OOH , cyclic ether formation is energetically more favorable than the competing β -scissions. Methoxymethoxy-1,3-dioxetane is formed in the case of Q_1OOH with an electronic barrier of 86.0 kJ mol^{-1} and methoxy-1,3,5-trioxane in the case of Q_3OOH with an electronic barrier of 82.0 kJ mol^{-1} . Due to the characteristic structure of OMEs, it is only possible to form cyclic ethers with an even number of atoms in the ring with equal amounts of oxygen and carbon atoms. Compared to Q_2OOH , the energy of the lowest activated transition states starting from Q_1OOH and Q_3OOH amount at least 30 kJ mol^{-1} more. Formed cyclic ethers decompose quickly via an elementary unimolecular reaction, as shown in **Eq. (2)** and **Eq. (3)**.



Cyclic ether formation is an exothermic reaction in which the reaction enthalpy depends on the formed ring structure and substituents, e.g., a four-ring introduces more ring strain than a six-ring which reduces the reaction enthalpy. The subsequent decomposition is highly exothermic in nature, during which two single carbon-oxygen bonds are each replaced with a double carbon-oxygen bond. Q_3OOH can also isomerize via a hydroxyl-shift with an electronic barrier of 83.8 kJ mol^{-1} , which competes with the cyclic ether formation. Oxy-radicals

decompose mainly via β -scission reactions with breaking of C-H bonds creating carbonyl functionalities as well. Quantum chemical calculations are not found for hydroxyl-shifts with a five-membered cyclic transition state.

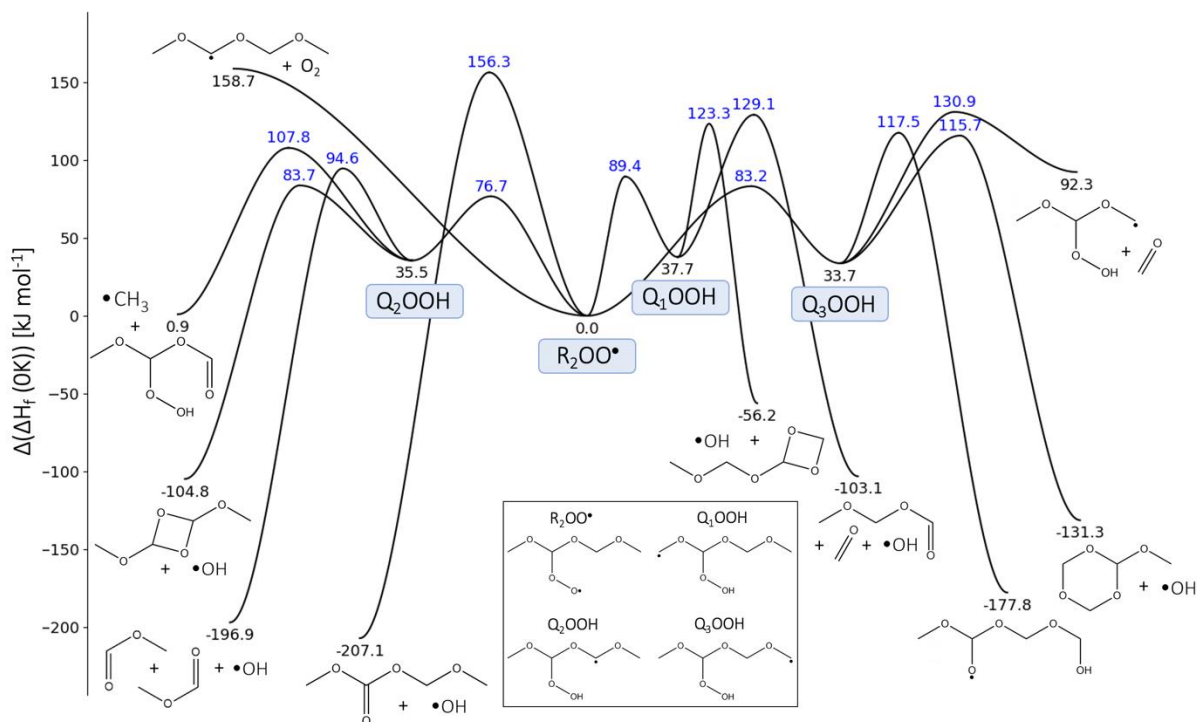


Fig. 5. Schematic partial potential energy surface for the addition of $R_2\cdot$ to molecular oxygen. The values are CBS-QB3 calculated enthalpies of formation at 0 K relative to the enthalpy of formation of $R_2OO\cdot$.

Results for $R_1OO\cdot$ are somewhat different (cf. **Fig. 6**). The most favorable intramolecular hydrogen abstraction after the addition of molecular oxygen is via an eight-membered transition state forming Q_5OOH (i.e., $HOOCOCOC\cdot OC$) with an electronic barrier of only 67.9 kJ mol^{-1} . For none of the hydroperoxy alkyl radicals the cyclic ether formation was found to be the energetically favorable reaction pathway. Instead, beta-scissions or intramolecular hydroxyl shifts have lower electronic barriers. Due to entropic contributions, being more important with increasing temperature, the cyclic ether formation still plays a role in the decomposition chemistry. The expected product spectrum is thus similar for the decomposition of $R_2OO\cdot$ and $R_1OO\cdot$, being mainly OME derived species with carbonyl functionalities.

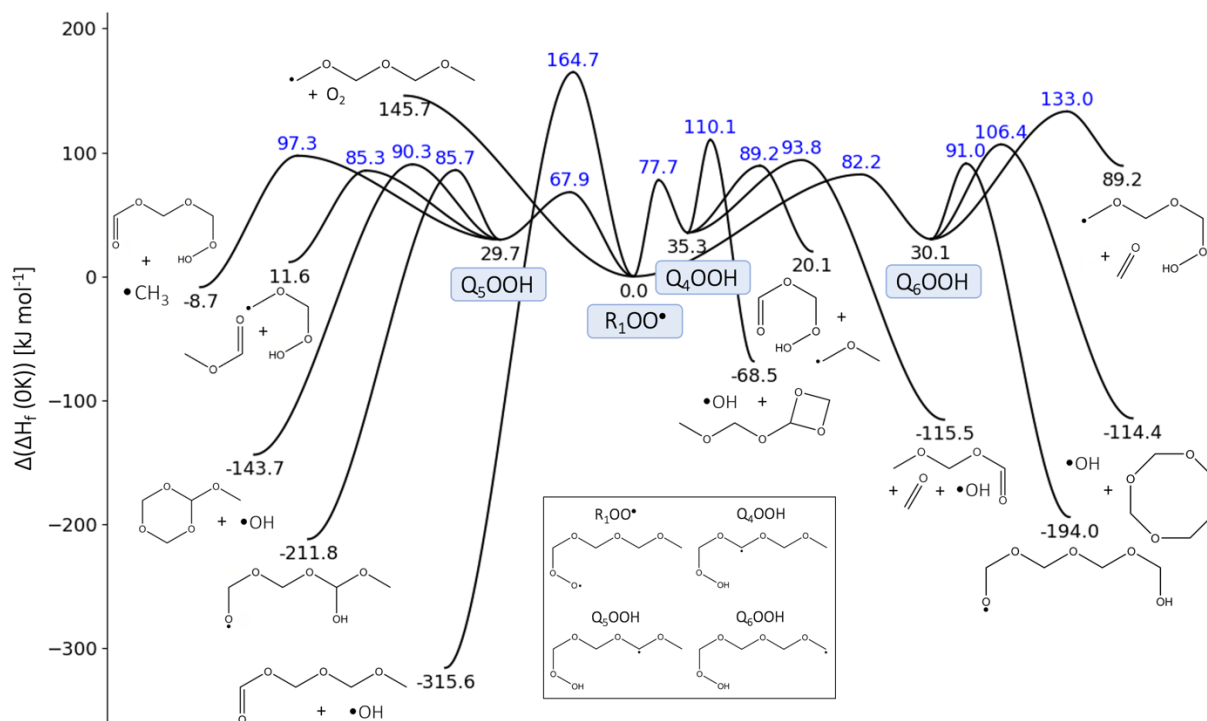
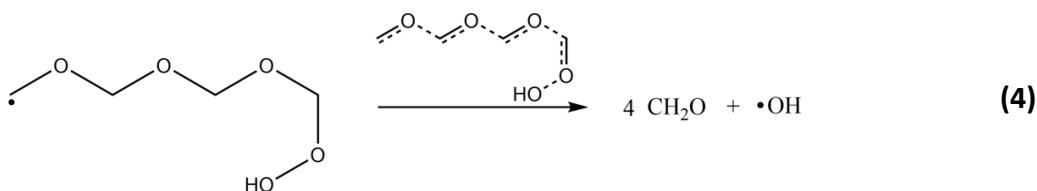


Fig. 6. Schematic partial potential energy surface for the addition of R_1^* to molecular oxygen. The values are CBS-QB3 calculated enthalpies of formation at 0 K relative to the enthalpy of formation of R_1OO^* .

An extra family of elementary reactions was found for the hydroperoxy alkyl radicals by combined homolytic scission of the hydroperoxide group and consecutive beta-scissions, as shown in Eq. (4) for $HOOCOCOCOC^*$. However, these reactions are not important since the corresponding electronic barriers exceed the electronic reaction enthalpy of the reverse dissociation reaction to molecular oxygen and R_1^* or R_2^* .



5.3. Experimental results and kinetic model simulations

Reactor simulations are performed with the newly developed kinetic model and compared with the experimentally acquired data. The results are described, first for the experiments on the micro-pyrolysis unit (low- and high-temperature pyrolysis) and then for the RCM unit (low-temperature oxidation). Validation with experimental data from literature, i.e., the ignition

delay times obtained from a shock tube (Cai et al. [19]) and an RCM (Drost et al. [24]), is provided in the **Supplementary Information**.

5.3.1. Low- and high-temperature pyrolysis

Reactor simulations are performed using CHEMKIN-PRO [50] with the developed kinetic model. The tubular reactor of the micro-pyrolysis unit is modeled as an ideal plug flow reactor (PFR). A discussion on the PFR assumption is provided in the **Supplementary Information**. The measured temperature profiles are imposed as input along the reactor. The inlet composition is calculated via the ideal gas law based on the average peak width of the feed pulse, the injected volume of OME-2 and the volumetric flow rate of helium. The mole fractions of the simulations of the continuous PFR effluent are compared with the molar composition of the batch experiments.

Fig. 7 depicts the experimental and model predicted mole fractions of OME-2 and major product species as a function of the temperature for the micro-pyrolysis experiments with the quartz tube reactor. The thermal decomposition of OME-2 starts slowly at around 500 K under oxygen-free conditions, enhances significantly at 800 K and reaches full conversion at 900 K. The detected oxygenated species are DMM, DME, formaldehyde, methoxymethyl formate, methoxymethanol, methyl formate, methanol, water, CO and CO₂, while other products are methane, ethane, ethylene and H₂. Overall, the developed kinetic model is able to predict the experimental trends, peak locations and concentrations of the major products satisfactorily.

With the decomposition of OME-2 being initiated, the concentrations of DMM and formaldehyde increase, reach a maximum with 6.0 mol% at 825 K and with 13.8 mol% at 900 K, respectively, after which these decrease rapidly. Around 800 K, a spectrum of oxygenated products starts to be formed, i.e., methanol, methyl formate, methoxymethyl formate, CO and CO₂. The formation of methane and H₂ is also initiated at 800 K. Methoxymethyl formate and methyl formate are the only OME derived compounds with a carbonyl functionality observed. The concentration of these intermediates increases with temperature and reaches a maximum at 850 and 900 K, respectively. Despite a multitude of products in the reacting system containing methoxy groups, the formation of methanol is minor reaching a maximum concentration of only 2.5 mol% at around 1000 K. The mole fractions of CO and H₂ continue to increase with temperature and do not reach a maximum; these are the major products formed at higher temperatures and seem to be correlated with each other. Contrary to DMM being an important product initially formed, DME is only detected in minor amounts (max 0.2 mol%) at higher temperatures after reaching full conversion of OME-2. The detected products containing carbon-carbon bonds are ethane and ethylene. The latter compounds could not be measured separately due to overlap in the chromatograms. There are no indications that products larger than OME-2 are effectively formed, e.g., by radical recombination reactions, during the thermal decomposition.

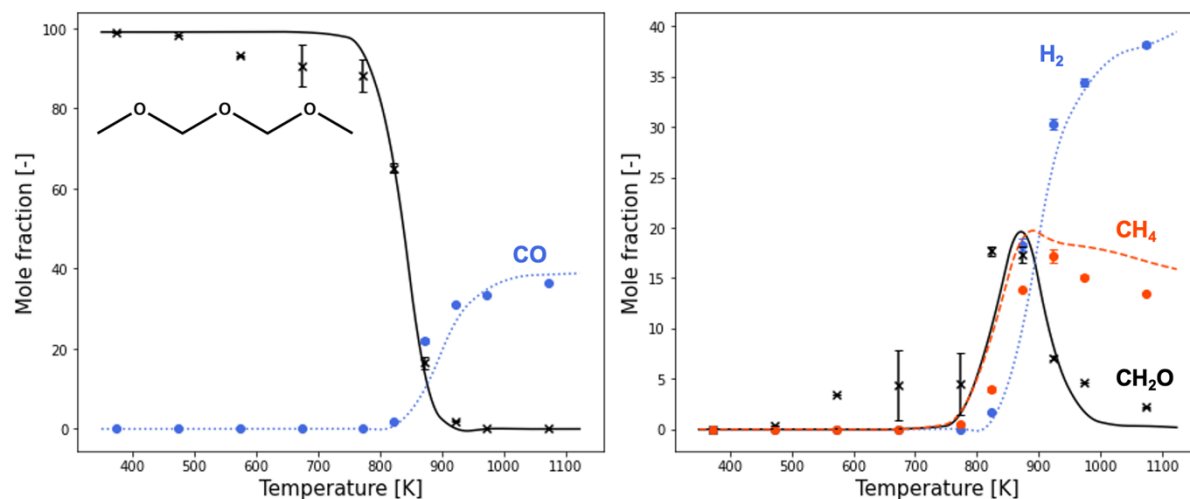


Fig. 7. Comparison between major products experimental (symbols) and model predicted (lines) mole fractions as a function of temperature for the pyrolysis of OME-2 in the quartz tube reactor of the micro-pyrolysis unit. Experimental conditions are a pressure of 0.34 MPa and injection of 0.3 μL OME-2 in a 92 Nml min^{-1} He stream. The product mole fractions are normalized excluding the He dilution.

5.3.2. Low-temperature oxidation

The measured (FS)IDTs are simulated using the core gas compression – expansion approach dedicated to take into account the compression phase and heat losses after compression using the measured volume profiles.

Fig. 8 presents the performance of the kinetic model to reproduce the measured FSIDTs and IDTs from the RCM unit. **Fig. 1** already compared measured pressure profiles and simulation results for auto-ignition by compression of an OME-2/air mixture to 1.0 MPa. A two-stage auto-ignition is observed. The first-stage of ignition becomes more pronounced at higher temperatures and lower pressures. Under the given reaction conditions, the evolution of IDTs with temperature deviates from an Arrhenius behavior. However, a negative temperature coefficient region is not observed. The model is able to predict well the experimental results as a function of the temperature. The effect of a different compression pressure is well captured in the model, but the FSIDT is underestimated at higher temperatures. At higher temperatures, the experimental results might be impacted by the compression phase, since the measured ignition delay times are very short and close to the commonly accepted lower limit of 2 ms for the measurement of RCM IDTs. From a modeling point of view at higher temperatures, no simulation result is possible for FSIDT because of reactivity during the compression phase whereby the T_c cannot be estimated accurately. A comparison between the performance of the newly developed model and the model developed by Cai et al. [19] to reproduce the experimental (FS)IDTs from the RCM is provided in the **Supplementary Information**.

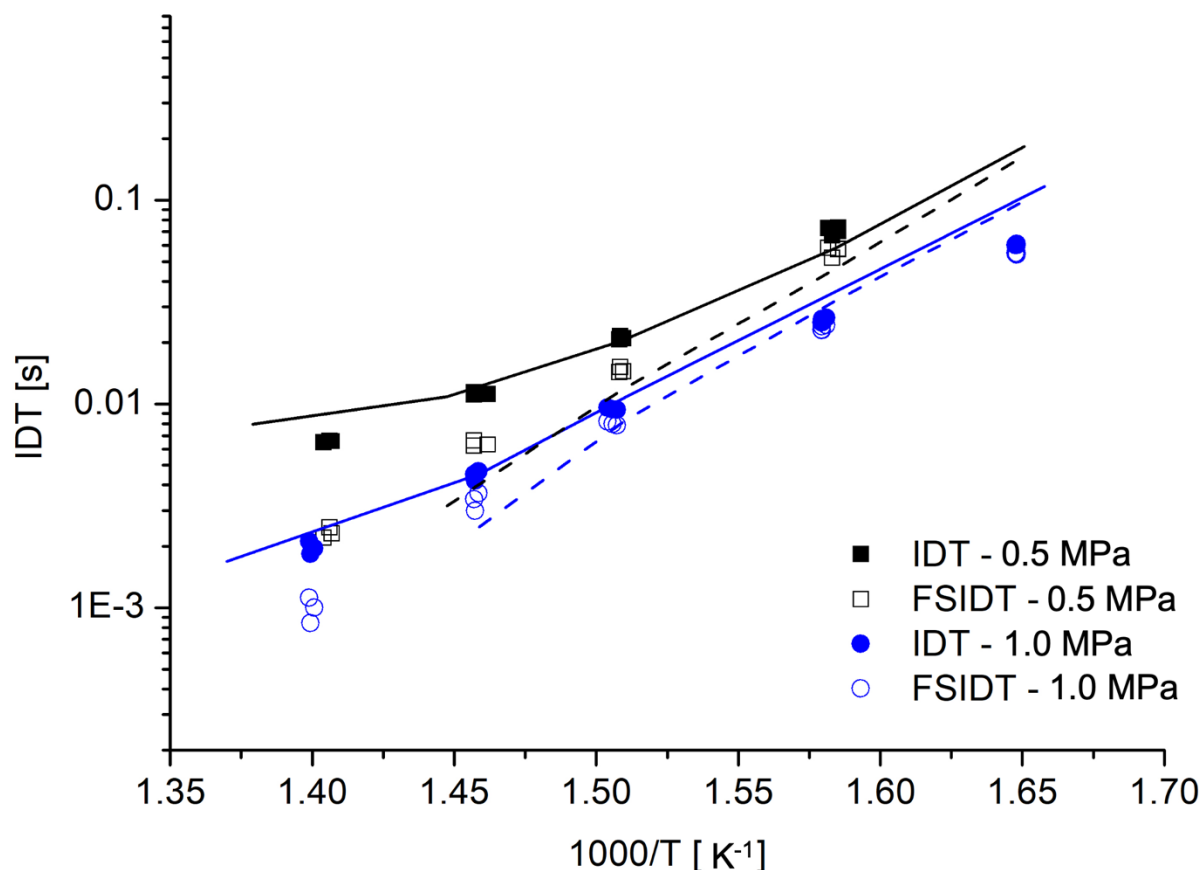


Fig. 8. Comparison between experimental first-stage (FSIDT) and total (IDT) ignition delay times (points) and simulation results (lines) in the ULille rapid compression machine for OME-2/air mixtures with an equivalence ratio ϕ of 0.5 for pressures of 0.5 (black) and 1.0 MPa (blue) and temperatures ranging from 600 to 715 K.

5.4. Pyrolysis reaction pathways

A rate of production analysis for the pyrolysis of OME-2 at 873 K and 0.34 MPa in the micro-pyrolysis unit for the quartz tube reactor is presented in **Fig. 9** for two points along the reactor. Highlighted species are detected experimentally. The experimental conversion of OME-2 amounts to 83 % at the reactor outlet for this condition. The predicted conversion by the model at 3.00 and 7.08 cm in the reactor amounts to 1% and 62%, respectively. At 3.00 cm in the reactor, the temperature of the reactant flow is still increasing and equals 830 K.

The OME-2 consumption is dominated by both the formaldehyde elimination reaction and hydrogen abstractions. Radicals originate mainly from the roaming reaction forming methoxymethanol and methoxycarbene, which decomposes into the formyl and methyl radicals. The contribution of all homolytic scission reactions is an order of magnitude smaller than the roaming reaction. Despite radical chemistry taking place, the formaldehyde elimination reaction remains important along the reactor. At 873 K, the formed DMM is not

Fig. 9. Rate of production analysis for pyrolysis of OME-2 at 873 K and 0.34 MPa in the micro-pyrolysis unit with the quartz tube reactor. Percentages report the rate of production relative to the production of the indicated reactant at a distance of 3.0 cm (bold numbers) and 7.08 cm (underlined numbers) in the reactor. Species that are detected experimentally are highlighted.

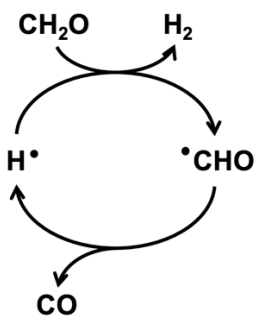


Fig. 10. Decomposition cycle from formaldehyde to CO and H₂.

5.5. Low-temperature oxidation reaction pathways

A rate of production analysis for the low-temperature oxidation of a fuel-lean air/OME-2 mixture in the ULille RCM unit for a pressure of 0.5 MPa and T_c 663 K is shown in **Fig. 11**. The analysis is performed for the first-stage ignition at a fuel consumption of 10% and the total ignition at a fuel consumption of 50%.

OME-2 is in both cases completely consumed by hydrogen abstractions. For the first-stage ignition, most of the hydrogen abstractions are by the hydroxyl radical, which shifts to both the hydroxyl and hydroperoxyl radical for the total ignition. Hydrogen abstraction forming R_2^\bullet is favored similarly as during pyrolysis. The formed radical can either undergo β -scission or the addition of molecular oxygen. For both stages, this β -scission is the dominant decomposition pathway. Only for the first-stage ignition some molecular oxygen adds after which the formed radical undergoes an internal hydrogen abstraction forming another secondary carbon radical. This hydroperoxy alkyl radical mainly decomposes by one β -scission although the cyclic ether formation has the lowest electronic barrier, see **section 5.2**. The pathways look different for R_1^\bullet for which the molecular oxygen addition is dominant during the first-stage ignition. The formed peroxy radical rearranges via two internal hydrogen abstractions forming the secondary carbon radicals which decompose by β -scissions. During total ignition, the temperature has risen whereby the molecular oxygen addition to R_1^\bullet becomes less important. The molecular rearrangement to R_2^\bullet and the β -scission forming formaldehyde and the methoxymethoxymethyl radical are equally important for R_1^\bullet during total ignition.

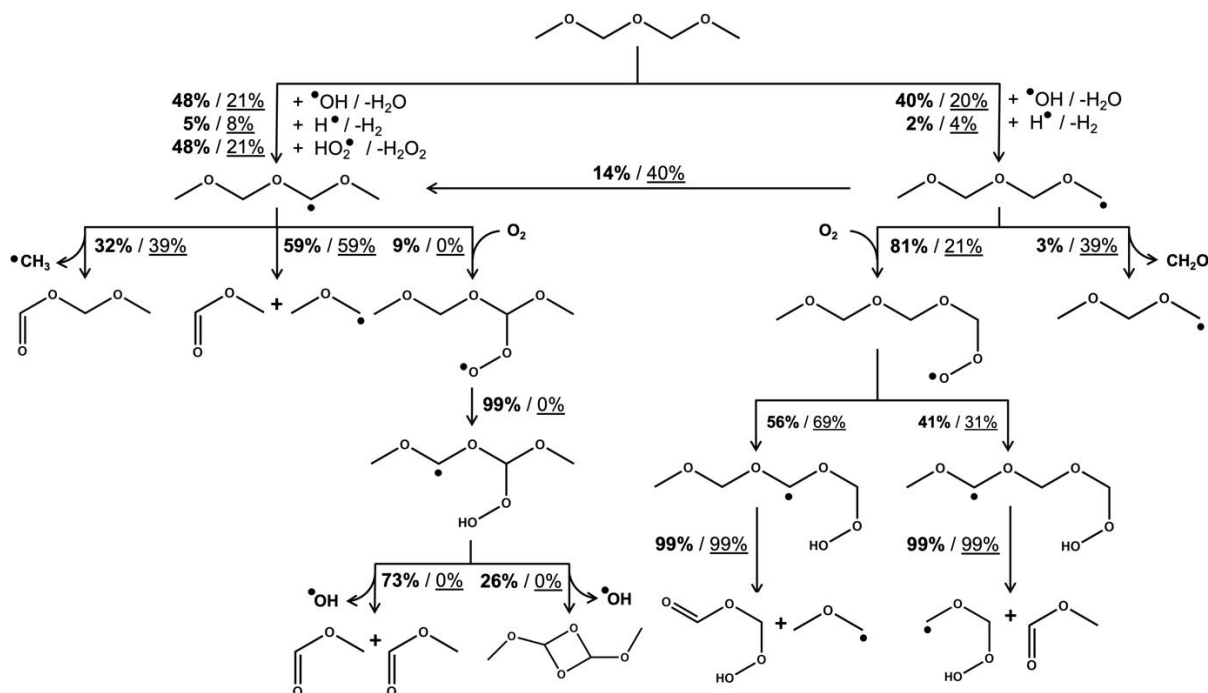


Fig. 11. Rate of production analysis for the low-temperature oxidation in the RCM unit with a 1.9 mol% OME-2, 19.61 mol% O₂ and 78.43 mol% N₂ mixture (equivalence ratio ϕ of 0.5), pressure of 0.5 MPa and Tc of 663 K. Numbers represent normalized fluxes at 10 % of fuel consumption during the first-stage of ignition (bold) and normalized fluxes at 50% of fuel (underlined).

The model is also validated against the experimental data from Cai et al. [19] and Drost et al. [24] (see the **Supplementary Information**), covering both low- and intermediate-temperature oxidation conditions. Model predictions agree well with the experimental results, except for the fuel-lean condition (ϕ equals 0.5) in a shock tube where an overprediction of the reactivity is observed between 700 and 950 K. This might be due to the absence of the addition of hydroperoxy alkyl radicals to molecular oxygen in the model which will be subject to future research.

5.6. Sensitivity analyses

Sensitivity analyses are performed to better understand the importance of reaction pathways responsible for the consumption of OME-2. In the presented sensitivity analyses, a positive sensitivity coefficient for a given reaction indicates that increasing the associated pre-exponential factor will reduce the decomposition of OME-2. Analogously, a negative sensitivity coefficient for a given reaction indicates that increasing the associated pre-exponential factor will enhance the decomposition of OME-2.

5.6.1. Pyrolysis

The sensitivity analysis with respect to the mole fraction of OME-2 for pyrolysis in the micro-pyrolysis unit for 873 K and 0.34 MPa at 3.00 and 7.08 cm along the reactor is presented in **Fig. 12**. Most of the sensitive reactions are fuel-specific reactions. The consumption is very sensitive towards the formaldehyde elimination reaction and the hydrogen abstraction by the methyl radical both in the beginning and at the end of the reactor. Also, the roaming reaction with formation of the methoxycarbene and methoxymethanol is a very sensitive reaction since it is the major production source of radicals. The recombination of two methyl radicals to form ethane has a negative sensitivity coefficient since it reduces the number of radicals in the reaction environment. The favored hydrogen abstraction from a secondary carbon atom is also reflected in a higher sensitivity coefficient for the associated reactions compared to the primary carbon atom.

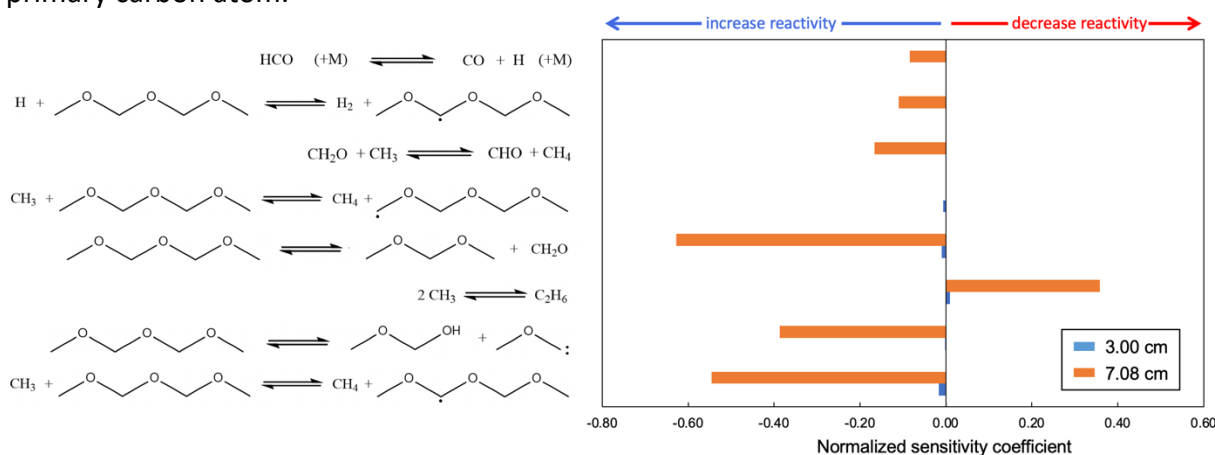


Fig. 12. Normalized sensitivity coefficients on the mole fraction of OME-2 during OME-2 pyrolysis. Experimental conditions correspond to a pressure of 0.34 MPa and a temperature of 873 K at 3.00 (blue) and 7.08 cm (orange) along the second reactor (quartz tube reactor) of the micro-pyrolysis unit.

5.6.2. Low-temperature oxidation

The brute force sensitivity analysis results with respect to the mole fraction of OME-2 for the ignition delay time experiments in the ULille rapid compression machine unit for 0.5 MPa and an equivalence ratio ϕ of 0.5 are shown in **Fig. 13**. Only the hydrogen abstractions by hydroxyl radicals are sensitive. The abstraction leading to R_2^{\cdot} decreases the reactivity while the abstraction forming R_1^{\cdot} increases the reactivity. R_2^{\cdot} is only partly undergoing addition of molecular oxygen and mostly β -scission reaction which does not form reactive hydroxyl radicals. This is different for R_1^{\cdot} where a large fraction reacts with molecular oxygen, which will form hydroperoxyl groups leading to hydroxyl radicals. Therefore, also the isomerization from R_1^{\cdot} to R_2^{\cdot} is a sensitive reaction which leads to inhibition of the OME-2 decomposition. Other important reactions which have an increasing effect on the reactivity are related to the

developed to describe the pyrolysis and oxidation chemistry based on quantum chemical derived thermodynamic parameters and reaction rate coefficients for important species and reactions, respectively. The model can predict the experimental trends of the pyrolysis and oxidation well without adjustment of reaction rates or thermodynamic parameters. The addition of hydroperoxy alkyl radicals to molecular oxygen is not included in the model which could possibly explain discrepancies with experimental data from a shock tube for larger oxygen concentrations. The fundamental knowledge obtained from the OME-2 chemistry can now be extrapolated to construct detailed kinetic models for larger OMEs that are eligible for fuel (additive) applications.

Supplementary Information

Main Word document (.docx) containing the characteristics of the GC × GC analyses and oven settings, the OME-2 feed pulse distribution in the micro-pyrolysis reactor, the temperature profiles in the micro-pyrolysis reactor, the validation against shock tube experiments (Cai et al. [19]) and rapid compression machine experiments (Drost et al. [24]), justification of the ideal plug flow reactor model assumption for the micro-pyrolysis reactor and a comparison between the performance of the model from Cai et al. and our newly developed model for the acquired rapid compression machine data. This main SI document also outlines the content of 12 additional files and their designations, which contain the experimental results from the micro-pyrolysis unit and rapid compression machine unit in a separate Excel file (.xlsx), a second Word document (.docx) containing the quantum chemical results, the developed kinetic model for OME-2 in CHEMKIN format (.inp) and the measured volume history profiles for each condition (10 in total) stored in a separate file (.csv).

Declaration of Competing Interest

The authors declare that they have no known competing financial interests or personal relationships that could have appeared to influence the results reported in this paper.

Acknowledgments

This work was established in a joint call to strengthen collaboration between I-SITE Université Lille Nord-Europe (members and national partners) and Ghent University. The computational resources and services used in this work were provided by the VSC (Flemish Supercomputer Center), funded by the Fund for scientific Research Flanders (FWO) and the Flemish Government department EWI. Kevin De Ras and Ruben Van de Vijver acknowledge the Fund for Scientific Research Flanders (FWO) for financial support via doctoral fellowship grant 3F018119 and post-doctoral fellowship grant 3E013419, respectively. The research leading to these results has also received funding from the European Research Council under the European Union's Horizon 2020 research and innovation programme / ERC grant agreement n° 818607. This work is a contribution to the CPER research project CLIMIBIO. The authors from PC2A thank the French Ministère de l'Enseignement Supérieur et de la Recherche, the

Hauts-de-France Region and the European Funds for Regional Economical Development for their financial support to this project.

References

- [1] S. Deutz, D. Bongartz, B. Heuser, A. Kätelhön, L. Schulze Langenhorst, A. Omari, M. Walters, J. Klankermayer, W. Leitner, A. Mitsos, S. Pischinger, A. Bardow, Cleaner production of cleaner fuels: wind-to-wheel – environmental assessment of CO₂-based oxymethylene ether as a drop-in fuel, *Energy & Environmental Science* 11 (2018) 331-343.
- [2] K. De Ras, R. Van de Vijver, V.V. Galvita, G.B. Marin, K.M. Van Geem, Carbon capture and utilization in the steel industry: challenges and opportunities for chemical engineering, *Current Opinion in Chemical Engineering* 26 (2019) 81-87.
- [3] D. Bongartz, J. Burre, A. Mitsos, Production of Oxymethylene Dimethyl Ethers from Hydrogen and Carbon Dioxide—Part I: Modeling and Analysis for OME₁, *Industrial & Engineering Chemistry Research* 58 (2019) 4881-4889.
- [4] A. Omari, B. Heuser, S. Pischinger, C. Rüdinger, Potential of long-chain oxymethylene ether and oxymethylene ether-diesel blends for ultra-low emission engines, *Applied Energy* 239 (2019) 1242-1249.
- [5] J. Liu, H. Wang, Y. Li, Z. Zheng, Z. Xue, H. Shang, M. Yao, Effects of diesel/PODE (polyoxymethylene dimethyl ethers) blends on combustion and emission characteristics in a heavy duty diesel engine, *Fuel* 177 (2016) 206-216.
- [6] Z. Wang, H. Liu, J. Zhang, J. Wang, S. Shuai, Performance, Combustion and Emission Characteristics of a Diesel Engine Fueled with Polyoxymethylene Dimethyl Ethers (PODE₃₋₄)/ Diesel Blends, *Energy Procedia* 75 (2015) 2337-2344.
- [7] H. Liu, X. Wang, Y. Wu, X. Zhang, C. Jin, Z. Zheng, Effect of diesel/PODE/ethanol blends on combustion and emissions of a heavy duty diesel engine, *Fuel* 257 (2019) 116064.
- [8] B. Lumpp, D. Rothe, C. Pastötter, R. Lämmermann, E. Jacob, Oxymethylene ethers as diesel fuel additives of the future, *MTZ worldwide eMagazine* 72 (2011) 34-38.
- [9] D. Pélerin, K. Gaukel, M. Härtl, E. Jacob, G. Wachtmeister, Potentials to simplify the engine system using the alternative diesel fuels oxymethylene ether OME₁ and OME₃₋₆ on a heavy-duty engine, *Fuel* 259 (2020) 116231.
- [10] K. Vertin, J. Ohi, D. Naegeli, K. Childress, G. Hagen, C. McCarthy, A.S. Cheng, R. Dibble, Methylal and Methylal-Diesel Blended Fuels from Use In Compression-Ignition Engines, *SAE Technical Papers*, 1999.
- [11] J. Burger, M. Siegert, E. Ströfer, H. Hasse, Poly(oxymethylene) dimethyl ethers as components of tailored diesel fuel: Properties, synthesis and purification concepts, *Fuel* 89 (2010) 3315-3319.
- [12] F.H. Vermeire, H.-H. Carstensen, O. Herbinet, F. Battin-Leclerc, G.B. Marin, K.M. Van Geem, Experimental and modeling study of the pyrolysis and combustion of dimethoxymethane, *Combust. Flame* 190 (2018) 270-283.
- [13] L. Golka, I. Weber, M. Olzmann, Pyrolysis of dimethoxymethane and the reaction of dimethoxymethane with H atoms: A shock-tube/ARAS/TOF-MS and modeling study, *Proc. Combust. Inst.* 37 (2019) 179-187.
- [14] W.A. Kopp, L.C. Kröger, M. Döntgen, S. Jacobs, U. Burke, H.J. Curran, K. Alexander Heufer, K. Leonhard, Detailed kinetic modeling of dimethoxymethane. Part I: Ab initio thermochemistry and kinetics predictions for key reactions, *Combust. Flame* 189 (2018) 433-442.

- [15] S. Jacobs, M. Döntgen, A.B.S. Alqaity, W.A. Kopp, L.C. Kröger, U. Burke, H. Pitsch, K. Leonhard, H.J. Curran, K.A. Heufer, Detailed kinetic modeling of dimethoxymethane. Part II: Experimental and theoretical study of the kinetics and reaction mechanism, *Combust. Flame* 205 (2019) 522-533.
- [16] L. Marrodán, E. Royo, Á. Millera, R. Bilbao, M.U. Alzueta, High Pressure Oxidation of Dimethoxymethane, *Energy & Fuels* 29 (2015) 3507-3517.
- [17] Y. Zhu, C.-W. Zhou, A.A. Konnov, Combustion chemistry of methoxymethanol. Part I: Chemical kinetics of hydrogen-abstraction reactions and the unimolecular reactions of the product [C₂H₅O₂] radicals, *Combust. Flame* 229 (2021) 111396.
- [18] A.A. Konnov, E.J.K. Nilsson, M. Christensen, C.-W. Zhou, Combustion chemistry of methoxymethanol. Part II: Laminar flames of methanol+formaldehyde fuel mixtures, *Combust. Flame* 229 (2021) 111411.
- [19] L. Cai, S. Jacobs, R. Langer, F. vom Lehn, K.A. Heufer, H. Pitsch, Auto-ignition of oxymethylene ethers (OMEn, n = 2–4) as promising synthetic e-fuels from renewable electricity: shock tube experiments and automatic mechanism generation, *Fuel* 264 (2020) 116711.
- [20] T. He, Z. Wang, X. You, H. Liu, Y. Wang, X. Li, X. He, A chemical kinetic mechanism for the low- and intermediate-temperature combustion of Polyoxymethylene Dimethyl Ether 3 (PODE3), *Fuel* 212 (2018) 223-235.
- [21] W. Sun, G. Wang, S. Li, R. Zhang, B. Yang, J. Yang, Y. Li, C.K. Westbrook, C.K. Law, Speciation and the laminar burning velocities of poly(oxymethylene) dimethyl ether 3 (POMDME3) flames: An experimental and modeling study, *Proc. Combust. Inst.* 36 (2017) 1269-1278.
- [22] Y. Zhao, N. Li, Y. Xie, Y. Cheng, X. Wang, Study on chemical kinetic mechanisms of Polyoxymethylene Dimethyl Ethers (PODEn), *IOP Conference Series: Materials Science and Engineering* 768 (2020) 022056.
- [23] Y. Fenard, G. Vanhove, A Mini-Review on the Advances in the Kinetic Understanding of the Combustion of Linear and Cyclic Oxymethylene Ethers, *Energy & Fuels* 35 (2021) 14325-14342.
- [24] S. Drost, R. Schießl, M. Werler, J. Sommerer, U. Maas, Ignition delay times of polyoxymethylene dimethyl ether fuels (OME2 and OME3) and air: Measurements in a rapid compression machine, *Fuel* 258 (2019) 116070.
- [25] N.M. Vandewiele, K.M. Van Geem, M.-F. Reyniers, G.B. Marin, Genesys: Kinetic model construction using chemo-informatics, *Chemical Engineering Journal* 207-208 (2012) 526-538.
- [26] G. SriBala, R. Van de Vijver, L. Li, O. Dogu, G.B. Marin, K.M. Van Geem, On the primary thermal decomposition pathways of hydroxycinnamic acids, *Proc. Combust. Inst.* 38 (2021) 4207-4214.
- [27] S.P. Pyl, C.M. Schietekat, K.M. Van Geem, M.-F. Reyniers, J. Vercaemmen, J. Beens, G.B. Marin, Rapeseed oil methyl ester pyrolysis: On-line product analysis using comprehensive two-dimensional gas chromatography, *Journal of Chromatography A* 1218 (2011) 3217-3223.
- [28] H. Song, R. Dauphin, G. Vanhove, A kinetic investigation on the synergistic low-temperature reactivity, antagonistic RON blending of high-octane fuels: Diisobutylene and cyclopentane, *Combust. Flame* 220 (2020) 23-33.

- [29] Y. Fenard, M.A. Boumehdi, G. Vanhove, Experimental and kinetic modeling study of 2-methyltetrahydrofuran oxidation under engine-relevant conditions, *Combust. Flame* 178 (2017) 168-181.
- [30] S.S. Goldsborough, S. Hochgreb, G. Vanhove, M.S. Wooldridge, H.J. Curran, C.-J. Sung, Advances in rapid compression machine studies of low- and intermediate-temperature autoignition phenomena, *Progress in Energy and Combustion Science* 63 (2017) 1-78.
- [31] M.J. Frisch, G.W. Trucks, H.B. Schlegel, G.E. Scuseria, M.A. Robb, J.R. Cheeseman, G. Scalmani, V. Barone, G.A. Petersson, H. Nakatsuji, X. Li, M. Caricato, A.V. Marenich, J. Bloino, B.G. Janesko, R. Gomperts, B. Mennucci, H.P. Hratchian, J.V. Ortiz, A.F. Izmaylov, J.L. Sonnenberg, Williams, F. Ding, F. Lipparini, F. Egidi, J. Goings, B. Peng, A. Petrone, T. Henderson, D. Ranasinghe, V.G. Zakrzewski, J. Gao, N. Rega, G. Zheng, W. Liang, M. Hada, M. Ehara, K. Toyota, R. Fukuda, J. Hasegawa, M. Ishida, T. Nakajima, Y. Honda, O. Kitao, H. Nakai, T. Vreven, K. Throssell, J.A. Montgomery Jr., J.E. Peralta, F. Ogliaro, M.J. Bearpark, J.J. Heyd, E.N. Brothers, K.N. Kudin, V.N. Staroverov, T.A. Keith, R. Kobayashi, J. Normand, K. Raghavachari, A.P. Rendell, J.C. Burant, S.S. Iyengar, J. Tomasi, M. Cossi, J.M. Millam, M. Klene, C. Adamo, R. Cammi, J.W. Ochterski, R.L. Martin, K. Morokuma, O. Farkas, J.B. Foresman, D.J. Fox, Gaussian 16 Rev. C.01, Wallingford, CT, 2016.
- [32] A.L.L. East, L. Radom, Ab initio statistical thermodynamical models for the computation of third-law entropies, *The Journal of Chemical Physics* 106 (1997) 6655-6674.
- [33] L.A. Curtiss, K. Raghavachari, P.C. Redfern, J.A. Pople, Assessment of Gaussian-2 and density functional theories for the computation of enthalpies of formation, *The Journal of Chemical Physics* 106 (1997) 1063-1079.
- [34] G.A. Petersson, D.K. Malick, W.G. Wilson, J.W. Ochterski, J.A.M. Jr., M.J. Frisch, Calibration and comparison of the Gaussian-2, complete basis set, and density functional methods for computational thermochemistry, *The Journal of Chemical Physics* 109 (1998) 10570-10579.
- [35] C.A.R. Pappijn, F.H. Vermeire, R. Van de Vijver, M.-F. Reyniers, G.B. Marin, K.M. Van Geem, Bond additivity corrections for CBS-QB3 calculated standard enthalpies of formation of H, C, O, N, and S containing species, *International Journal of Chemical Kinetics* 53 (2021) 345-355.
- [36] C. Eckart, The Penetration of a Potential Barrier by Electrons, *Physical Review* 35 (1930) 1303-1309.
- [37] P.D. Paraskevas, M.K. Sabbe, M.-F. Reyniers, N. Papayannakos, G.B. Marin, Group Additive Values for the Gas-Phase Standard Enthalpy of Formation, Entropy and Heat Capacity of Oxygenates, *Chemistry – A European Journal* 19 (2013) 16431-16452.
- [38] NIST Chemistry WebBook. <https://webbook.nist.gov/>.
- [39] H.-H. Carstensen, A.M. Dean, Rate Constant Rules for the Automated Generation of Gas-Phase Reaction Mechanisms, *The Journal of Physical Chemistry A* 113 (2009) 367-380.
- [40] H.-H. Carstensen, A.M. Dean, A quantitative kinetic analysis of CO elimination from phenoxy radicals, *International Journal of Chemical Kinetics* 44 (2012) 75-89.
- [41] A.G. Vandeputte, M.K. Sabbe, M.-F. Reyniers, V. Van Speybroeck, M. Waroquier, G.B. Marin, Theoretical Study of the Thermodynamics and Kinetics of Hydrogen Abstractions from Hydrocarbons, *The Journal of Physical Chemistry A* 111 (2007) 11771-11786.
- [42] R. Van de Vijver, N.M. Vandewiele, P.L. Bhoorasingh, B.L. Slakman, F. Seyedzadeh Khanshan, H.-H. Carstensen, M.-F. Reyniers, G.B. Marin, R.H. West, K.M. Van Geem, Automatic

Mechanism and Kinetic Model Generation for Gas- and Solution-Phase Processes: A Perspective on Best Practices, Recent Advances, and Future Challenges, *International Journal of Chemical Kinetics* 47 (2015) 199-231.

[43] M. Saeys, M.-F. Reyniers, G.B. Marin, V. Van Speybroeck, M. Waroquier, Ab initio group contribution method for activation energies for radical additions, *AIChE Journal* 50 (2004) 426-444.

[44] P.D. Paraskevas, M.K. Sabbe, M.-F. Reyniers, N.G. Papayannakos, G.B. Marin, Group Additive Kinetics for Hydrogen Transfer Between Oxygenates, *The Journal of Physical Chemistry A* 119 (2015) 6961-6980.

[45] L. Cai, H. Pitsch, S.Y. Mohamed, V. Raman, J. Bugler, H. Curran, S.M. Sarathy, Optimized reaction mechanism rate rules for ignition of normal alkanes, *Combust. Flame* 173 (2016) 468-482.

[46] J. Bugler, K.P. Somers, E.J. Silke, H.J. Curran, Revisiting the Kinetics and Thermodynamics of the Low-Temperature Oxidation Pathways of Alkanes: A Case Study of the Three Pentane Isomers, *The Journal of Physical Chemistry A* 119 (2015) 7510-7527.

[47] W.K. Metcalfe, S.M. Burke, S.S. Ahmed, H.J. Curran, A Hierarchical and Comparative Kinetic Modeling Study of C1 – C2 Hydrocarbon and Oxygenated Fuels, *International Journal of Chemical Kinetics* 45 (2013) 638-675.

[48] T. Panaget, N. Mokrani, S. Batut, A. Lahcen, Y. Fenard, L. Pillier, G. Vanhove, Insight into the Ozone-Assisted Low-Temperature Combustion of Dimethyl Ether by Means of Stabilized Cool Flames, *The Journal of Physical Chemistry A* 125 (2021) 9167-9179.

[49] M. Döntgen, W.A. Kopp, F. vom Lehn, L.C. Kröger, H. Pitsch, K. Leonhard, K.A. Heufer, Updated thermochemistry for renewable transportation fuels: New groups and group values for acetals and ethers, their radicals, and peroxy species, *International Journal of Chemical Kinetics* 53 (2021) 299-307.

[50] R.J. Kee, F.M. Rupley, E. Meeks, J.A. Miller, CHEMKIN-III: A FORTRAN chemical kinetics package for the analysis of gas-phase chemical and plasma kinetics, Sandia National Lab. (SNL-CA), Livermore, CA (United States), 1996.